INTERFACE

rsif.royalsocietypublishing.org

Research

Cite this article: Dai L, He G, Zhang X, Zhang X. 2018 Stable formations of self-propelled fish-like swimmers induced by hydrodynamic interactions. *J. R. Soc. Interface* **15**: 20180490. http://dx.doi.org/10.1098/rsif.2018.0490

Received: 29 June 2018
Accepted: 19 September 2018

Subject Category:
Life Sciences–Physics interface

Subject Areas:
biomechanics, biomimetics

Keywords:
biolocomotion, fluid–structure interaction, computational fluid dynamics, fish schooling, energy efficiency

Author for correspondence:
Xing Zhang
e-mail: zhangx@lnm.imech.ac.cn

Electronic supplementary material is available online at https://dx.doi.org/10.6084/m9.figshare.c.4254073.

THE ROYAL SOCIETY PUBLISHING

Stable formations of self-propelled fish-like swimmers induced by hydrodynamic interactions

Longzhen Dai[1,2], Guowei He[1,2], Xiang Zhang[1,2] and Xing Zhang[1,2]

[1]The State Key Laboratory of Nonlinear Mechanics, Institute of Mechanics, Chinese Academy of Sciences, Beijing 100190, People's Republic of China
[2]School of Engineering Science, University of Chinese Academy of Sciences, Beijing 100049, People's Republic of China

LD, 0000-0002-7337-9942; XZ, 0000-0002-4960-0221

Fish schools are fascinating examples of macro-scale systems with collective behaviours. According to conventional wisdom, the establishment and maintenance of fish schools probably need very elaborate active control mechanisms. Sir James Lighthill posited that the orderly formations in fish schools may be an emergent feature of the system as a result of passive hydrodynamic interactions. Here, numerical simulations are performed to test Lighthill's conjecture by studying the self-propelled locomotion of two, three and four fish-like swimmers. We report the emergent stable formations for a variety of configurations and examine the energy efficiency of each formation. The result of this work suggests that the presence of passive hydrodynamic interactions can significantly mitigate the control challenges in schooling. Moreover, our finding regarding energy efficiency also challenges the widespread idea in the fluid mechanics community that the diamond-shaped array is the most optimized pattern.

1. Introduction

Collective behaviours of self-propelled objects immersed in fluid have recently become a trans-disciplinary research focus which has attracted attention from biologists, physicists, applied mathematicians and engineers. Examples of the systems studied include insect swarms [1,2], fish schools [3,4], bird flocks [5–7], bacteria swarms [8,9] and assemblies of active micro-particles [10,11]. To date, most of the works were concerned with micro-scale systems. From the perspective of fluid mechanics, understanding collective behaviours in macro-scale systems is more challenging due to the complexity associated with increased Reynolds number.

Fish schools represent one typical example of macro-scale systems with emergent collective behaviours. The study of the fish schooling phenomenon has a long history in zoology and ethology [3]. This fascinating phenomenon also inspired the development of theoretical models by physicists and mathematicians [12–15]. Despite the past efforts, two riddles remain unsolved. First, what is the reason for the aggregation of a large number of fish? Second, how do fish maintain the orderly patterns during swimming?

To answer the first question, several reasons have been suggested. The possibilities include social and genetic factors [16], reducing predation [17,18], advantages in feeding [19] and also energy benefits due to hydrodynamic factors [13,14,20,21]. With regard to the benefits of swimming in schools, the diamond pattern was once thought to be the most optimized pattern for reducing energy expenditure [13,14]. Although the experimental evidence to support this was largely lacking and some contradictory results have been obtained in natural systems [22,23], this is still the most widespread idea in the fluid mechanics community. In a recently study, other patterns

such as line, phalanx and rectangle, were also found to enjoy some hydrodynamic advantages over solitary swimming [24].

As to the second question, the conventional view is that fish are smart enough to subtly tune their swimming gaits to position themselves at the preferred locations in perturbed flows. Thus, the synchronized swimming in fish schools may require complex collective decision and feedback control mechanisms [25]. Following this philosophy, some computational models for two tandem fish in a sustained 'leader–follower' configuration have been developed recently. In these works, the optimized swimming gaits of the follower were selected via minimizing expended power [26] or reinforcement learning [27,28].

In this regard, a rather different view was proposed by Sir James Lighthill in the 1970s [29]. He posited that the orderly patterns can spontaneously emerge and remain stable with the aid of 'passive forces' that originate from the flow-mediated interactions. He also drew an analogy between the grouping of fish and the formation of crystals by liquid molecules. The hypothesis that 'passive forces facilitate the coordinated grouping of swimming fish' is termed the Lighthill conjecture. Although it is theoretically elegant, this scientific hypothesis has been barely touched for a long time (neither proved nor disproved).

Recently, some progress has been made with respect to the Lighthill conjecture. Several numerical and experimental studies were carried out to investigate the interactions between two self-propelled swimmers in a 'leader–follower' configuration [30–32]. Both swimmers were modelled as flapping foils with prescribed heaving motions and self-propulsion was permitted in the horizontal direction. The results indicated that the hydrodynamic interactions alone were sufficient to generate coordinated collective locomotion. If both swimmers were independently actuated, the inter-spacing was also found to be dynamically determined [30,32].

The above works shed some light on the critical role that 'passive forces' have played in the grouping of active swimmers. However, the scenarios considered in those works were very dissimilar to that of fish schooling. First, fish use wave-like undulations to propel themselves forward, while the kinematics of the swimmers in those studies somewhat resembled those observed in the flapping wings of birds. Second, only the 'leader–follower' configuration of two swimmers was examined. It is thus not clear whether those results can be extended to more complex configurations.

In the present work, we explore the validity of the Lighthill conjecture by using a computational model which bears a closer resemblance to the fish schooling problem than the ones used in [30–32]. More specifically speaking, we study the schooling of two, three and four self-propelled fish-like swimmers and examine the emergent stable formations for the in-line, side-by-side and staggered configurations. The present study is a natural extension of [30] but it is also significantly different from it. We believe that it represents one important step forward towards a full understanding of the role that hydrodynamic interactions play in the establishment and maintenance of fish schools. Besides, the results of this study can also provide useful insight into the control of unmanned underwater vehicle (UUV) formations.

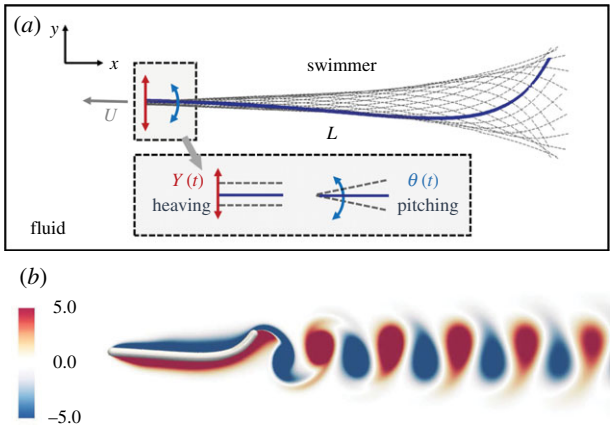

Figure 1. An FSI-driven swimmer which emulates a fish performing undulatory locomotion: (*a*) schematic diagram for the computational model; (*b*) wake structure represented by the vorticity contours. (Online version in colour.)

2. Computational model and methodology

2.1. Computational model

A thin elastic filament is used as a proxy for a fish performing undulatory locomotion (figure 1*a*). The swimmer is actuated by the prescribed sinusoidal heaving and pitching motions at its head. The specific forms of the vertical displacement and the rotating angle imposed at the head are $y(t) = y_0 + A\cos(2\pi ft + \phi)$ and $\theta(t) = \theta_0\cos(2\pi ft + \phi - \pi/2)$, respectively. Here y_0 is the equilibrium lateral position of the heaving motion, f is the actuation frequency, A and θ_0 are the heaving and pitching amplitudes, ϕ is the phase angle. To ensure free swimming, the horizontal displacement of the head is not constrained.

The self-propelled swimming of the filament is governed by the two-dimensional incompressible Navier–Stokes equations, together with the nonlinear dynamics equations. The governing equations for the fluid flow can be written in a dimensionless form as

$$\frac{\partial \boldsymbol{u}}{\partial t} + (\boldsymbol{u}\cdot\nabla)\boldsymbol{u} = -\nabla p + \frac{1}{Re}\nabla^2\boldsymbol{u} + \boldsymbol{f} \tag{2.1a}$$

and

$$\nabla\cdot\boldsymbol{u} = 0, \tag{2.1b}$$

where $\boldsymbol{u}$ is the velocity vector and p is the pressure, $\boldsymbol{f}$ is the forcing term which represents the effect of the immersed body on the flow. Re is the flapping Reynolds number which is defined as $Re = (U_{\mathrm{ref}}L)/\nu$, where U_{ref}, L and ν are the reference velocity, the length of the filament and the kinetic viscosity of the fluid, respectively. Here the reference velocity is chosen to be the maximum trailing edge velocity for a *rigid* filament when only the sinusoidal *pitching* motion is imposed at the leading edge, i.e. $U_{\mathrm{ref}} = 2\pi\theta_0 fL$.

The physical meaning of the Reynolds number is the ratio of inertial force over viscous force. In some references, the Reynolds number based on the swimming velocity is also used. The swimming Reynolds number and the flapping Reynolds number are usually of the same order in magnitude and proportional to each other. In the realm of Reynolds numbers typical of adult fish swimming, the inertial forces are dominant and viscous forces are negligible (i.e. $Re \gg 1$).

The governing equations for the motion of the flexible filament can be written in a dimensionless form as

$$\beta(s)\frac{\partial^2 \boldsymbol{X}}{\partial t^2} - \frac{\partial}{\partial s}\left(\xi(s)\frac{\partial \boldsymbol{X}}{\partial s}\right) + \frac{\partial^2}{\partial s^2}\left(\gamma(s)\frac{\partial^2 \boldsymbol{X}}{\partial s^2}\right) = -\boldsymbol{F} \qquad (2.2a)$$

and

$$\frac{\partial \boldsymbol{X}}{\partial s}\cdot\frac{\partial \boldsymbol{X}}{\partial s} = 1, \qquad (2.2b)$$

where $\mathbf{X}$ is the position vector, s is the Lagrangian coordinate along the arc length, $\boldsymbol{F}$ is the Lagrangian forcing term due to interactions with the fluid. In the framework of the immersed boundary method for solving the coupled fluid-and-structure system, the forcing terms $\boldsymbol{f}$ and $\boldsymbol{F}$ are two forms of the interaction force between the filament and the ambient fluid. $\boldsymbol{f}$ and $\boldsymbol{F}$ can be transformed from one form to the other by using an interpolation kernel function [33].

The mass ratio β, the dimensionless tension coefficient ξ and the dimensionless bending rigidity γ are defined as $\beta = (\rho_s\delta)/(\rho_f L)$, $\xi = T/(\rho_f U_{ref}^2 L)$ and $\gamma = B/(\rho_f U_{ref}^2 L^3)$, respectively. Here ρ_s and ρ_f are the densities of the filament and the fluid respectively, δ is the thickness of the filament, T and B are the (dimensional) tension coefficient and the (dimensional) bending rigidity of the filament. In this work, β, ξ and γ are functions of s and not constants. $\xi(s)$ is governed by a Poisson-type equation which can be used to enforce the inextensible constraint (equation (2.2*b*)) on the filament [33]. $\beta(s)$ and $\gamma(s)$ are two exponential decay functions which will be given later in subsection 2.2.

Superficially, the computational model here looks too simplified and remote from the real problem of fish schooling. However, some important key elements of the real problem are still retained in the model. It can thus serve as the starting point for the investigations of more complicated systems. More explanations are provided here on the connections between this model and the real problem.

The motion of the swimmer's body is driven by the fluid–structure interaction (FSI). This passive elastic mechanism is completely different from the internal actuation mechanism in fish swimming. However, in this work, hydrodynamic interaction (rather than actuation) is the only focus and the primary factor that determines the hydrodynamics is the body kinematics. Thus, the model problem bears a close resemblance to the real one, as long as the swimming gaits are similar. The desired swimming gait is reproduced by tuning the material properties rather than directly prescribing the deformation. The reasons for such practice are as follows. First, as a natural extension of [30], a similar actuation mechanism is adopted in the present study. Second, the passive mechanism has been extensively used in the previous studies [34–36]. The studies on the relation between swimming gait and rigidity in these works can be very helpful in determining the values of some parameters. Third, it has been verified experimentally that the passive actuation mechanism in fish played an important role when swimming in a perturbed flow (such as the flow behind a cylinder) [37].

The frozen degrees of freedom (i.e. lateral displacement and rotation), which are inherited from [30], pose a great limitation to the present model. However, we believe that the permission of free swimming in the streamwise direction is already one big step forward. Since the pioneering work of Weihs [13], most models were built by fixing the swimmers' positions and placing them in a uniform stream. The only exceptions were references [30–32], in which the in-line configuration was studied without any constrains on the streamwise motions. The present work represents another important step forward by extending the results of [30] to fish-like swimmers and more complicated configurations.

The two-dimensional model is a considerable simplification of a three-dimensional school by looking only at one horizontal layer of fish. An assumption is first made such that the finite vortex sheets from each layer are combined into the infinite sheets along the depth. These vortex sheets are then assumed to roll up into two-dimensional arrays of vortices [13,14]. The assumptions above have been verified experimentally for fish swimming in shallow water (which is a mathematical equivalence to a single-layer school) [38]. In addition, some experiments were recently conducted to study the stable configurations for fish schooling in shallow water tunnels [39,40]. In this study, we aim to apply the present results to fish schooling in shallow water, such as the experiments of [39] and [40]. Moreover, the comparison of the present results with the analytic solutions from [13,14] can also help us gain some new insight into the problem.

2.2. Control parameters

Since most schooling fish are carangiform swimmers, here we attempt to emulate the carangiform gait on the filament. To achieve this aim, the mass ratio β and the dimensionless bending rigidity γ are assumed to exponentially decay from the head to the tail and are expressed by two exponential decay functions as

$$\beta(s) = a_1 e^{-b_1 s^m} \qquad (2.3a)$$

and

$$\gamma(s) = a_2 e^{-b_2 s^n}. \qquad (2.3b)$$

The coefficients in equations (2.3*a*) and (2.3*b*) are determined such that (i) the ranges of β and γ and are comparable with those of some biological propulsors [41–43]; (ii) the constraint $b_2 = 3b_1$ is satisfied and (iii) a carangiform swimming gait similar to that of the red nose tetra fish [39] is produced. The relation between b_1 and b_2 in (ii) can be derived as follows. Here we assume that the variations of β and γ along the body are caused solely by *non-uniformity* in the thickness δ. Since $\beta \propto \delta$ and $\gamma \propto \delta^3$, we have $\gamma \propto \beta^3$. From the exponential distributions depicted by equations (2.3*a*) and (2.3*b*), $b_2 = 3b_1$ is easily derived (provided that $m = n$ holds).

The parameters for controlling the decaying rates of these two quantities are determined through a cut-and-try procedure by regarding the swimming gait of red nose tetra fish *Hemigrammus bleheri* as the object for mimicking. The reason for choosing this particular type of fish is the availability of experimental data for the schooling patterns [39]. The values of all coefficients in the exponential decay functions are listed in table 1, and the resulting ranges of β and γ are 5×10^{-3}–0.1 and 1.2×10^{-4}–1.0, respectively.

The swimming gait of the artificial swimmer is obtained by numerically solving the FSI problem, under the values of the control parameters listed in table 1. After the steady locomotion state is reached, we compare the swimming gait of the artificial swimmer with that of the red nose tetra fish provided in [39]. It is found that the two swimming gaits possess similarities in the tail-beating amplitude, the ratio of wavelength to body length, the wave propagation speed,

Table 1. Values of the control parameters used in the simulations.

parameters	values
flapping Reynolds number ($U_{ref}L/\nu$)	600[a]
dimensionless heaving amplitude (A/L)	0.005
pitching amplitude (θ_0)	5°
coefficients in the exponential decay functions $\beta(s) = a_1 e^{-b_1 s^m}$ and $\gamma(s) = a_2 e^{-b_2 s^n}$	
a_1	0.1
b_1	3.0
m	2.0
a_2	1.0
b_2	9.0
n	2.0

[a]The Reynolds number defined by the swimming speed, the body length and the kinematic viscosity of the fluid is roughly 440.

etc. (see electronic supplementary material, figure S1 and table S1, for detailed comparisons). The Reynolds number defined by the swimming speed, the body length and the viscosity of the fluid is roughly 440, which is lower by no more than one order of magnitude when comparing with the Reynolds number range of 1000–6000 measured in the experiments of [39]. The wake structure produced by the fish-like swimmer is shown in figure 1*b* and a reversed Karman vortex street of '2S' wake mode (two vortices per flapping cycle) is clearly seen. This is the typical 'footprint' left behind by an inertial swimmer in fluid.

2.3. Material and methods

We use the immersed boundary method in the framework of the discrete stream-function formulation to solve the two-dimensional incompressible Navier–Stokes equations [44,45]. The algebraic multigrid method is used to solve the linear systems arising from the discretization. The computer code is parallelized using the message passing interface protocol [46]. The dynamics equations for the elastic filament are solved by using the finite difference method on a staggered grid. We use the loosely coupled method to handle the two-way interaction between the fluid flow and the motion of the filament [33]. This code has been thoroughly validated by using a variety of benchmark cases and the results match well with those from the references [33,44–46].

A rectangular computational domain with the size of $[-30L, 30L] \times [-6L, 6L]$ is used in the simulations. The no-slip boundary condition is enforced at the four boundaries, which are at least $5L$ away from the swimmers during swimming. This domain size is sufficiently large to minimize the artefacts caused by the unphysical blocking of the far-field boundaries [47]. The no-slip condition on the surface of the swimmer is realized by using the immersed boundary technique. For solving the dynamic equations of the filament, the free-end condition is enforced at the tail. As to the boundary condition imposed at the head, the horizontally free swimming condition is combined with the prescribed heaving and pitching motions [33]. Together with the dynamic equation which governs the motion of the filament, a Poison-type equation for the tension coefficient is also solved to enforce the inextensible constraint on the filament [48].

A multiblock Cartesian grid with hanging nodes is used for discretizing the Navier–Stokes equations. This grid contains six sub-grids with different levels of refinement, with a total cell number of 2.2 million. The mesh spacings are $0.16L$ and $0.005L$, for the coarsest and finest sub-grids, respectively (electronic supplementary material, figure S2). The grid for discretizing the dynamics equation has a uniform spacing of $0.005L$. The time step used in the simulations are selected such that the maximum *Courant–Friedrichs–Lewy* (*CFL*) number never exceeds 0.5.

To test the convergence of the solutions to the refinement of grids, solitary swimming of the elastic filament with the control parameters listed in table 1 is simulated by using three different mesh resolutions. The detailed information for the meshes used are listed in the electronic supplementary material, table S2. The time histories of the instantaneous swimming speed of the elastic filament, obtained at different mesh resolutions are shown in the electronic supplementary material, figure S3. The convergence behaviour of the instantaneous swimming speed with the refinement of mesh can be clearly seen. Apparent difference exists between the results obtained at $h = L/100$ and $h = L/200$. As the mesh is further refined to $h = L/300$, only a minor difference in the instantaneous swimming speed can be detected. To be more specific, the percentage difference in the results obtained at $h = L/300$ and $h = L/200$ is only 3.8%. As a compromise between the accuracy and the cost of computation, all simulations in this work are conducted at the resolution of $h = L/200$.

3. Results

3.1. Emergent stable formations

We now examine the collective swimming of two, three and four 'fish'. In these fish schools, all individuals are assumed to possess the same body size and also synchronize in one common longitudinal direction (i.e. the negative x direction which is also the swimming direction). The flapping frequencies and amplitudes for all individuals are the same (and also the same as those for a solitary swimmer). Several configurations, namely, the in-line, side-by-side and staggered arrangements of two fish, the side-by-side and staggered arrangements of three fish and the rectangular and diamond-shaped arrangements of four fish, are considered here.

In these arrangements, the lateral spacing between any two individuals in one school is prescribed as 0 or d, while the phase difference between any two individuals is set to 0 or π. The range of lateral spacing considered here is $0.15L \leq d \leq 0.65L$. The minimum and maximum values of d are determined by considering the following three factors. First, there is some biological evidence that the preferred lateral spacing in fish schools lies in the range of $0.16L$ to $0.6L$ (electronic supplementary material, table S3). Second, collision with the lateral neighbours is observed in some simulation cases if $d < 0.15L$. Third, if $d > 0.65L$, we find that stable formations are not achievable within the limited swimming distance (roughly $45L$) set by the size of the computational domain. To seek for all possible stable formations as best as we can, a variety of initial streamwise spacings are tried for each prescribed value of d (table 2). The stable formations can be clearly identified from the asymptotic behaviours in the time histories of streamwise spacing between individuals (some examples are shown in figure 2). Here we have to admit that some possible stable formations can still be left out despite the thorough search conducted.

In figure 3, the stable formations observed in the simulations are symbolized in a two-dimensional space. The

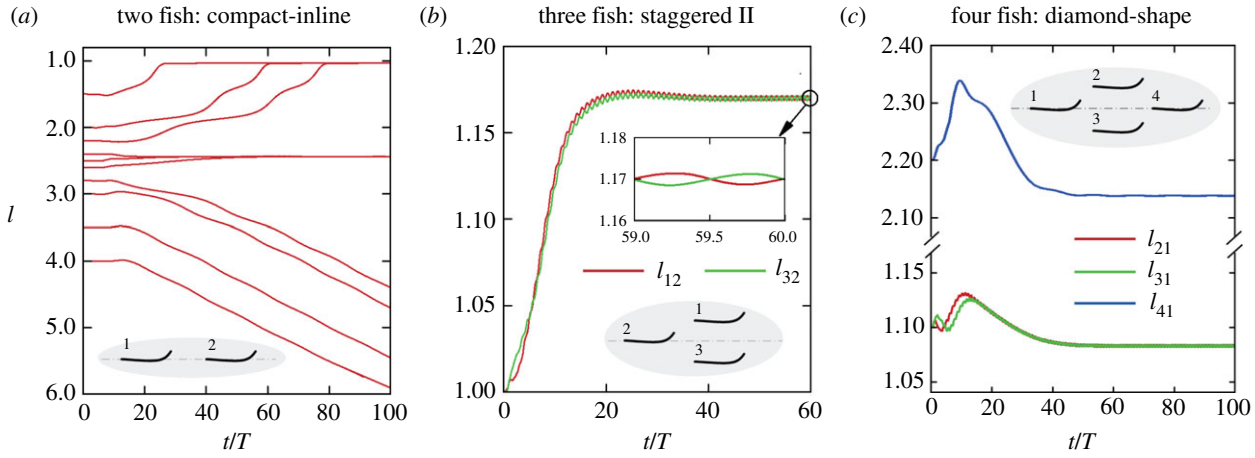

Figure 2. Time histories of the instantaneous streamwise distance *l* between the head of the reference fish and those of other fishes. (*a*) Two fish under the in-line pattern; (*b*) three fish under the staggered II pattern; (*c*) four fish under the diamond-shaped pattern. Please note from (*a*) that no stable in-line formations can be achieved if the initial separation distances are larger than 2.8*L*. (Online version in colour.)

Table 2. Values of lateral spacing and initial streamwise spacing for seeking the stable formations.

	lateral spacing (*L*)	initial streamwise spacing (*L*)	configuration type
two fish	0	1.5, 2.0, 2.2, 2.4, 2.5, 2.6, 2.8, 3.0, 3.5, 4.0	in-line
	0.2, 0.3, 0.4, 0.5, 0.6	1.1, 2.0	staggered
	0.15, 0.18, 0.2, 0.25, 0.3, 0.32, 0.35, 0.4, 0.5, 0.6	0	side-by-side (IP)
	0.3, 0.35, 0.4, 0.45, 0.5, 0.55, 0.6	0	side-by-side (AP)
three fish	0.25, 0.3, 0.35, 0.4, 0.5, 0.6, 0.65	0	side-by-side (IP)
	0.3, 0.35, 0.4, 0.45, 0.5, 0.55, 0.6	0	side-by-side (AP)
four fish	0.15, 0.2, 0.25	1.0, 1.1, 1.25	diamond-shaped
	0.5, 0.6	2.0, 2.5, 3.0, 3.5	rectangular

head position of one swimmer in each school (denoted by the stars in figure 3*a*) is placed at the origin in figure 3*b* and also denoted by a star. The head positions of other individuals in the same school are labelled by a variety of symbols. Please note that in the achieved stable formations, the streamwise spacings between any two individuals are *dynamically* determined and not prescribed.

The red solid circles represent the side-by-side formations of two fish with an anti-phase pattern. It is seen that no streamwise shifts are observed in these formations. The red open circles represent the side-by-side formations composed of two fish with an in-phase pattern. Among these formations, the largest streamwise shift of 0.12*L* is found at the lateral spacing of $d = 0.3L$. The flow structures corresponding to the side-by-side formations of two fish are shown in figure 4*a*,*b*.

The red pluses represent two possible in-line formations composed of two fish. The first one is the compact formation in which the two fish are almost in contact with each other (with a small gap distance of 0.04*L*). Thus, the two fish behave just like one elongated fish in solitary swimming. The second one is the loose formation in which the heads of two fish are approximately 2.44*L* apart. The flow structures corresponding to the two in-line formations are shown in figure 4*c*,*d*. Similar compact [30] and loose in-line formations [30,32] have also been found previously in the studies of two self-propelled rigid or slightly deformable flapping foils. This suggests that the emergence of stable formations is a generic feature of interacting active swimmers. In contrast with the two in-line formations found here, the existence of multiple stable in-line formations has been revealed in the studies of [30,32]. This implies that group cohesiveness of the in-line formations depends strongly on the swimming gaits adopted.

The red upward-facing triangles represent the staggered formations composed of two fish. Similar to the in-line formations, the staggered formations can also be categorized into the compact and loose types. The compact staggered formations are found at $d = 0.2L$ and $d = 0.3L$, with a streamwise shift of 1.04*L* (or a gap distance of 0.04*L*). The loose staggered formations are found at $d = 0.3L$ and $d = 0.4L$, with a streamwise shift of 1.92*L* (or a gap distance of 0.92*L*). The flow structures corresponding to the staggered formations of two fish are shown in figure 4*e*,*f* .

The blue solid circles represent the formations composed of three fish with an anti-phase pattern (the phase difference between lateral neighbours is π). It is seen that an exact side-by-side formation of three fish can only be achieved at the lateral spacing of 0.3*L*. For other lateral spacings, the upper and lower fish lead the middle fish in the streamwise direction. The maximum streamwise shift in this type of formations is approximately 0.10*L*, which is achieved at the lateral spacing of 0.6*L*. The blue open circles represent the side-by-side formations composed of three fish with an in-phase pattern. It is seen that the upper and lower fish

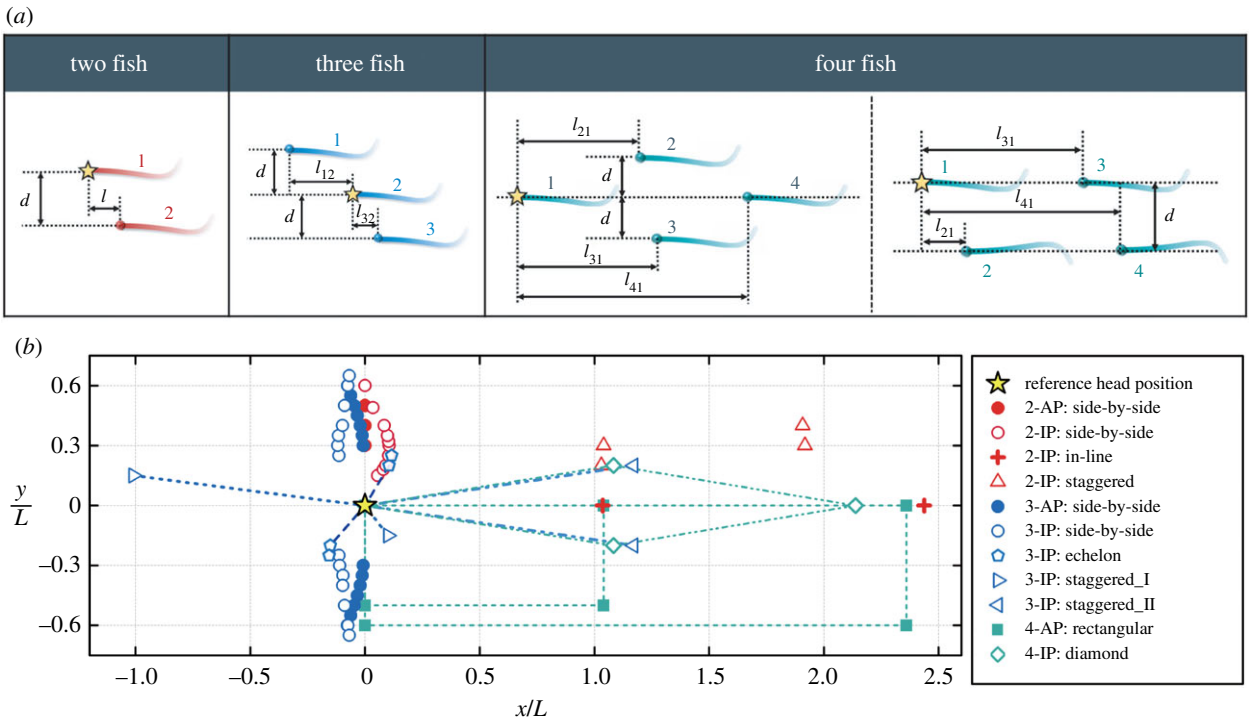

Figure 3. A diagram for the stable formations observed in the simulations: (*a*) different configurations considered in this work; (*b*) head positions of the fish in the stable formations. The head positions of the selected fish for each stable formation (denoted as a star in (*a*)) are placed at the origin in (*b*). The red, blue and cyan colours in (*b*) denote the fish head positions in the schools composed of two, three and four members, respectively. For visualizability, the three fish in the staggered and echelon formations, the four fish in the rectangular and diamond formations are connected by a variety types of lines. In the right inset of (*b*), 'IP' and 'AP' denote the in-phase mode and anti-phase mode, respectively.)

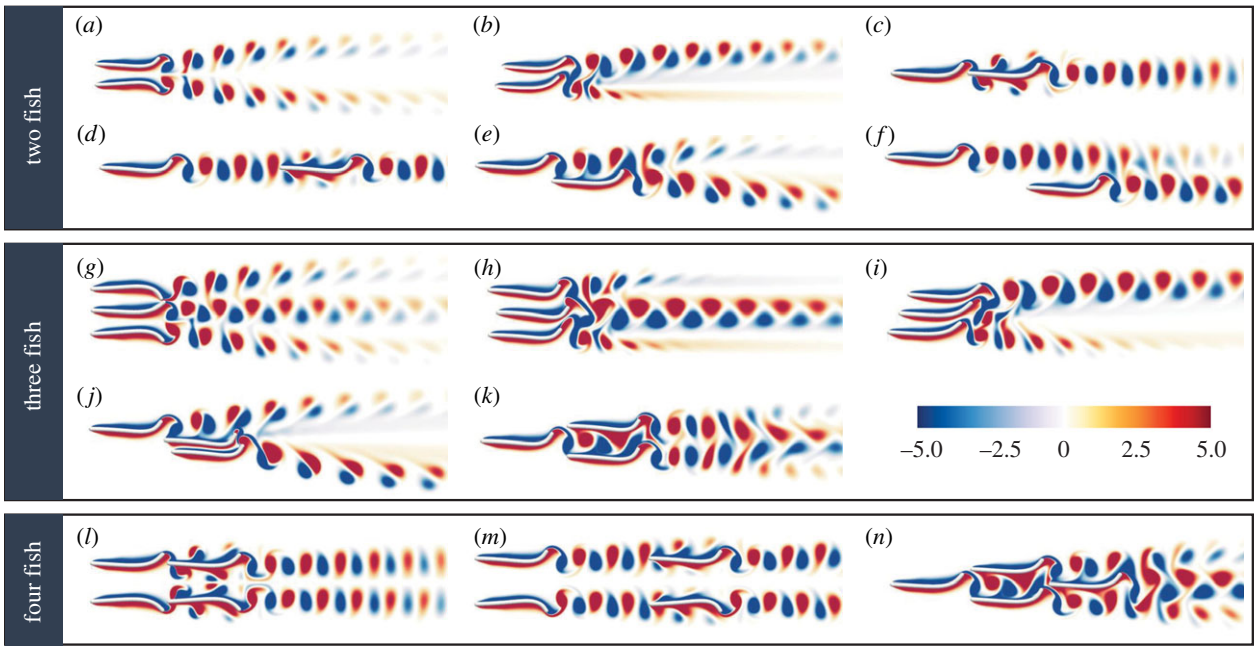

Figure 4. Flow structures represented by the vorticity contours for the stable formations composed of two, three and four fish: (*a*) two fish side-by-side (anti-phase); (*b*) two fish side-by-side (in-phase); (*c*) two fish in-line (compact); (*d*) two fish in-line (loose); (*e*) two fish staggered (compact); (*f*) two fish staggered (loose); (*g*) three fish side-by-side (anti-phase); (*h*) three fish side-by-side (in-phase); (*i*) three fish echelon; (*j*) three fish staggered (type I); (*k*) three fish staggered (type II); (*l*) four fish rectangular (compact, anti-phase); (*m*) four fish rectangular (loose, anti-phase); (*n*) four fish diamond. For all the formations listed here, the in-phase pattern is assumed if not specified. (Online version in colour.)

are exactly side-by-side while the middle fish lags behind in the streamwise direction. The largest streamwise shift between the middle fish and the upper (or the lower) fish is found to be $0.12L$, which is achieved at the lateral spacing of $d = 0.3L$. The flow structures corresponding to the side-by-side formations of three fish are shown in figure 4*g*,*h*.

The blue pentagons represent the echelon formations of three fish (with an in-phase pattern). In this type of

formations, the bottom fish is leading, while the middle and top ones lag behind in turn. The maximum streamwise shift between two lateral neighbours is 0.12*L*, which can be achieved at the lateral distance of 0.25*L*. The flow structure corresponding to the echelon formation is shown in figure 4*i*.

The blue rightward- and leftward-facing triangles represent the staggered formations composed of three fish (with an in-phase pattern). Type I staggered formation (denoted by the rightward-facing triangles) is achieved at the lateral spacing of 0.15*L*. In this type of formation, the top fish leads the middle one by roughly 1.0*L*, while the middle fish leads the bottom one by only 0.1*L*. Type II staggered formation (denoted by the leftward-facing triangles) is achieved at the lateral distance of 0.2*L*. In this type of formation, the middle fish leads the other two by roughly 1.15*L*. The flow structures corresponding to the staggered formations of three fish are shown in figure 4*j*,*k*.

The solid cyan squares represent the rectangular formation composed of four fish. Two possible stable formations of this type are found at the lateral spacings of 0.5*L* and 0.6*L*, respectively. The former can be categorized as the compact formation in the sense that the two in-line fish are only 0.04*L* apart from each other (this distance is the same as that in the compact in-line formation of two fish). The latter can be categorized as the loose formation in which the two in-line fish are 1.36*L* apart (this gap is slightly narrower than that of the loose in-line formation of two fish). The flow structures corresponding to the rectangular formations are shown in figure 4*l*,*m*.

The open cyan rhombuses represent the diamond-shaped formation composed of four fish with an in-phase pattern. This formation is only achieved at a lateral spacing of 0.2*L*. In this formation, one middle fish leads the two outer ones by 1.08*L*. These two outer fish are exactly side-by-side and also lead another middle fish by 1.08*L*. The corresponding flow structure for this formation is shown in figure 4*n*. It is interesting to note that the diamond formation observed here is more compact and shallower than the one proposed by Weihs [14], where the lateral spacing and streamwise spacings are 0.5*L* and 1.88*L*, respectively. Another interesting finding is that this diamond formation can only be achieved under the in-phase condition. (The diamond formation with an *anti-phase* pattern was suggested by Weihs [14], but such pattern is found to be unrealizable in the simulations.)

3.2. Energetics

The energy efficiency of the swimmers in the stable formations can be quantified by the cost of transport per unit mass (COT), which is defined as the energy required for a unit mass to travel a unit distance. COT is a dimensional quantity which is formally defined as

$$\mathrm{COT} = \frac{\bar{P}^*}{m\bar{U}^*}, \tag{3.1}$$

where $\bar{P}^*$ is the (*dimensional*) averaged input power, $\bar{U}^*$ is the (*dimensional*) averaged swimming speed, m is mass of the swimmer.

COT can also be expressed as

$$\mathrm{COT} = \frac{f^2 L}{\int_0^1 \beta(s)\,\mathrm{d}s} \cdot \frac{\bar{P}}{\bar{U}}, \tag{3.2}$$

where $\bar{P}$ and $\bar{U}$ are the *dimensionless* input power and the *dimensionless* averaged swimming speed, which are formally defined as

$$\bar{P} = \frac{1}{T_\mathrm{f}} \int_0^{T_\mathrm{f}} \int_0^1 [\boldsymbol{F}(s,t) \cdot \frac{\partial \boldsymbol{X}(s,t)}{\partial t}]\,\mathrm{d}s\,\mathrm{d}t \tag{3.3}$$

and

$$\bar{U} = \frac{1}{T_\mathrm{f}} \int_0^{T_\mathrm{f}} \frac{\partial X^1(0,t)}{\partial t}\,\mathrm{d}t. \tag{3.4}$$

Here X^1 denotes the x-component of the position vector $\boldsymbol{X}$, T_f is the dimensionless flapping period (i.e. $T_\mathrm{f} = 2\pi\theta_0$).

The relative difference of COT between a fish in formation swimming and that in solitary swimming can be computed as

$$\frac{\mathrm{COT} - \mathrm{COT_s}}{\mathrm{COT_s}} = \frac{(\bar{P}/\bar{U}) - (\bar{P}/\bar{U})_\mathrm{s}}{(\bar{P}/\bar{U})_\mathrm{s}}, \tag{3.5}$$

where the subscript 's' denotes solitary swimming.

The relative differences in COT of the swimmers in the stable formations and that of a solitary swimmer are shown in figure 5. It is seen that some formations can result in a noticeable enhancement in energy efficiency (i.e. reduction of COT), in comparison with that of a solitary swimmer. The formations with relatively large COT reductions are: (i) the side-by-side formations of two fish with an anti-phase pattern (figure 4*a*, up to 16% reduction); (ii) the compact rectangular formation of four fish (figure 4*l*, 14% reduction); (iii) the compact in-line formation of two fish (figure 4*c*, 14% reduction); (iv) the side-by-side formations of three fish with an anti-phase pattern (figure 4*g*, up to 13% reduction); (v) the type-I staggered formation of three fish (figure 4*j*, 11% reduction); (vi) the diamond-shape formation of four fish (figure 4*n*, 9% reduction); (vii) the compact staggered formation of two fish (figure 4*e*, 7% reduction). Please note that the values listed above are the percentages of COT reduction which are averaged among all members in the same school.

For other formations, the COT is almost the same as that of a solitary swimmer (the relative differences are within in the range of 5%). For example, in the loose in-line formation of two fish, almost no energetic advantages are gained. This is in contrast with the finding in [30], where the follower can enjoy up to 20% COT reduction in similar formations (which were composed of two self-propelled rigid or slightly deformable flapping foils). This implies that the energy efficiency in the loose in-line formations can be sensitive to the swimming gaits.

One finding that goes against our intuition is that the collective swimming does not always lead to an increased energy efficiency. For example, in the side-by-side formations with an in-phase pattern and also the echelon formation, the energy efficiencies are even lower than that of a solitary swimmer. Moreover, the finding of the present study also challenges the most widespread idea in the fluids mechanics community that the diamond-shaped formation is the most optimized schooling pattern [13,14]. It is manifest to us that the diamond formation does not show any energetic advantages over several other formations (such as the side-by-side formations with an anti-phase pattern).

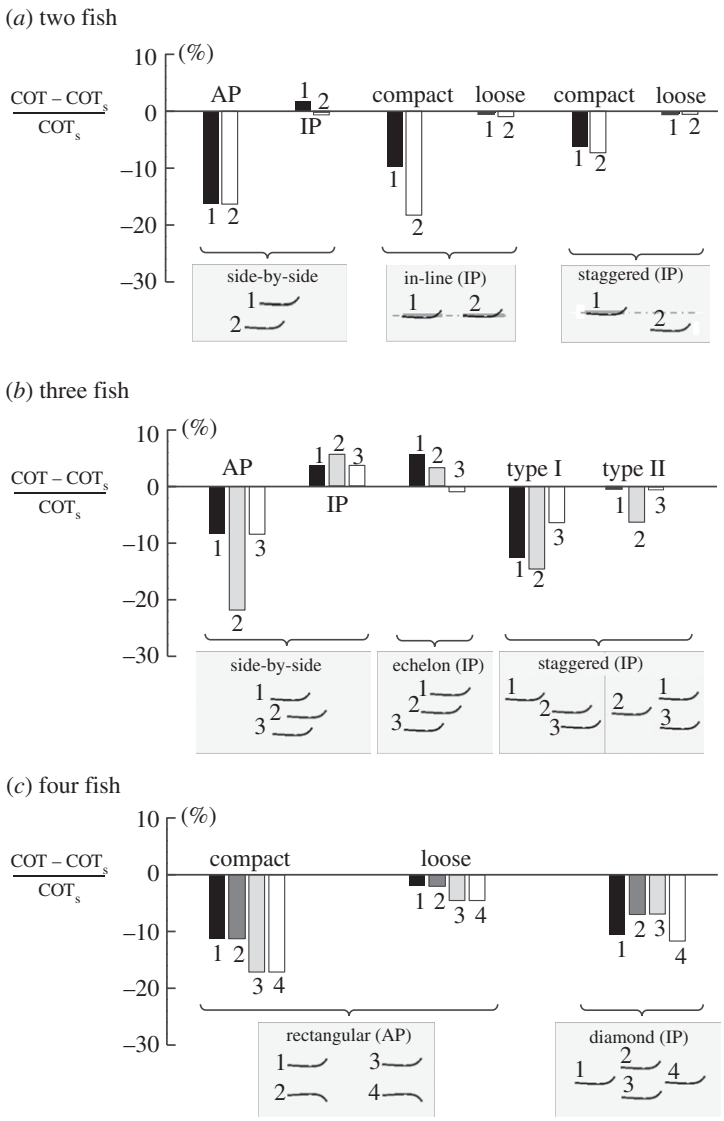

Figure 5. The relative differences in COT between those in formation swimming and that in solitary swimming: (*a*) two-fish formations; (*b*) three-fish formations; (*c*) four-fish formations. For the side-by-side and the echelon formations, the lowest COT among all possible lateral spacings is shown. COT_s denotes the COT in solitary swimming.

4. Discussion and conclusion

Our result suggests that multiple stable formations of the model fish school can be induced solely by hydrodynamic interactions. In the achieved stable formations, the settled streamwise positions are dynamically determined and are also the stable equilibrium points in terms of the streamwise hydrodynamic force. When perturbed, the hydrodynamic forces with significant strengths tend to restore the original positions [32]. For some individuals in certain formations, the prescribed lateral positions also happen to be the stable equilibrium points in terms of the lateral force or the torque. Thus, these swimmers can stay in their lateral positions (or maintain their longitudinal orientations) effortlessly. As one example, for the side-by-side formations of two fish with an anti-phase pattern, $d = 0.37L$ and $d = 0.32L$ are the two 'sweet-spots' in terms of the lateral force and the torque, respectively (electronic supplementary material, figure S4). Please note that these two 'sweet-spots' do not coincide with each other.

Generally speaking, the individuals in the stable formations can experience non-zero lateral force and/or torque if their lateral positions are not the 'sweet-spots' (such 'sweet-spots' may not even exist in some cases). Under such circumstances, counteracting measures are necessary for keeping the lateral positions and/or the body orientations. It is found that among all stable formations observed in the simulations, the magnitudes of lateral forces and torques are relatively small. The maximum lateral force and torque only reach up to 16% and 17% of the corresponding RMS values for a solitary swimmer (electronic supplementary material, table S4).

The simple strategies for maintaining a stable formation can thus be suggested as follows. First, all individuals synchronize in one common longitudinal orientation. Second, the actuation pattern which is the same as that of a solitary swimmer is adopted by all. Third, for fish, which mainly use bodies and caudal fins for propulsion, other fins can be used to produce small counteracting lateral forces and/or torques. One unresolved issue in justifying the strategies proposed here is whether all members can always manage to synchronize in one common longitudinal direction. Definite evidence has been found that fish can maintain a consistent heading and obtain guidance from an external reference (possibly related to the geomagnetic field) [49].

We can also argue that the ubiquity of unbalanced lateral forces and/or torques due to asymmetry only exists in schools of relatively small sizes. For larger schools, the 'sweet spots' can be easily found by the majority located in the interior portion, while the effect of asymmetry is only significant in the narrow region near the peripheries. Thus, counteracting forces and/or torques are only needed for the members located in this narrow region. One important implication of the arguments above is that lateral spacing is the parameter that can be fully controlled by the fish during schooling (unlike the streamwise spacing). The factors that determine the selection of a specific lateral spacing may include: (i) collision avoidance, (ii) force and/or torque balance and (iii) energy efficiency. For the majority in a large school, only (i) and (iii) are the main concerns.

Recently, possible biological evidence for 'passive hydrodynamic interactions facilitating fish grouping' has been discovered in the experiments on live fish. Ashraf *et al.* studied the collective swimming of two and three red nose tetra fish *Hemigrammus bleheri* in a shallow water channel [39]. This quasi-two-dimensional setting makes it easy for comparisons with the results of the present work. In their experiment, fish schools of side-by-side configurations with noticeable streamwise shifts (which resembles those shown in figure 4*b*,*h*,*i*) were observed. The presence of streamwise shifts in the formations was then rationalized by configuration optimization for maintaining a good transfer of information within the fish pairs [39]. Here we provide an alternative explanation: fish may rely on passive hydrodynamic interactions for grouping and the streamwise shifts are the emergent features of the system. In the experiments of [39], the streamwise spacing between the two fish in the side-by-side formations was measured around 0.16*L*. Intriguingly, the maximum streamwise spacing that is achievable in the present simulations is very close to this value (despite quite a few dissimilarities between the two systems, such as the actuation condition, the geometric shape and the Reynolds number). We also have to admit that a perfect one-to-one match between the swimming patterns found here and those observed in the experiment does not exist. Some formations shown in figure 4 never appear in the experiment of [39] and vice versa (electronic supplementary material, table S5). Presumably, the reason for the mismatch can be mainly attributed to the synchronization pattern in the lateral neighbours. In the present simulations, an in-phase or an anti-phase pattern is assumed (the phase difference is fixed to zero or π). However, in the experiment of [39], the periods of unsynchronization, in-phase synchronization and anti-phase synchronization in a fish pair are interspersed among each other.

Here, some attention is also paid to the selection of swimming formations in fish schools. A reasonable speculation is that under energy-demanding situations, maximizing the energy efficiency becomes the selection criterion. Some supporting evidence on this can be found in another experimental study by Ashraf *et al.* [40], where fish schools with up to nine members were examined. In this experiment, formations with large streamwise shifts among individuals were observed at their natural free swimming speed. The 'grouping units' in such schools resembled the patterns shown in figure 4*k*,*m*. At a much higher swimming speed, however, the side-by-side phalanx was the only formation observed. Moreover, the lateral neighbours in the phalanx tended to coordinate with each other in an in-phase or an anti-phase fashion and the lateral spacings between them also appeared to be much smaller than those in the formations observed at their natural free swimming speed.

From the perspective of energy efficiency, clearly, the anti-phase synchronization pattern is superior to the in-phase one. However, the lateral neighbours did not show a preference towards the anti-phase pattern in the side-by-side phalanx observed in [40]. (In the side-by-side formations of two fish and three fish observed at relatively high swimming speed [39], the anti-phase pattern was only slightly in favoured with respect to the in-phase pattern.) A plausible explanation for this phenomenon is still lacking.

It should be stressed, however, that even if the anti-phase pattern is only utilized intermittently [40], the side-by-side phalanx can still possibly outperform other formations in terms of energy efficiency. As can be inferred from the COT data shown in figure 5, in a side-by-side phalanx composed of large number of swimmers, the majority (except the ones at the top and the bottom of a school) may enjoy significant COT reductions provided that a proper lateral spacing is chosen (the COT reduction can reach up to 22% for the middle fish in a three-fish formation with an anti-phase pattern).

In this work, we provide a unique and somewhat contrarian view of how fish schools are established and maintained. We believe that the control challenges of schooling are significantly mitigated if fish can make the best use of the flow-mediated interactions. This view is against the conventional wisdom but is fully consistent with the picture of 'a school as a moving crystal of fish' proposed by Sir James Lighthill in the 1970s.

It should also be emphasized that the result of this study cannot rule out the possibility that fish may also resort to more complicated active control strategies for achieving some purposes such as maximizing compactness or energy efficiency of the schools. This explains the variety of configurations observed in fish schooling and the constant switching of positions within schools. In fact, the intricacies of fish schooling are far from being fully understood, especially when social behaviours are also involved. Thus, more in-depth studies (including experimental, theoretical and numerical ones) are still needed to eventually unveil this secret.

Data accessibility. This article has no additional data.

Authors' contributions. L.D., G.H. and Xi. Z. designed the research; L.D. performed the simulation; L.D., Xia. Z. and Xi. Z. wrote the code. L.D., G.H. and Xi. Z. wrote the paper.

Competing interests. The authors declare no conflict of interest.

Funding. This work was supported by Chinese Academy of Sciencesunder projects no. XDB22040104 and no. QYZDJ-SSW-SYS002; National Natural Science Foundation of Chinaunder project nos. 11772338, 11372331, 11232011 and 11572331; Ministry of Science and Technology of Chinaunder the 973 Program no. 2013CB834100.

Acknowledgements. We thank Professor D. Weihs for the helpful discussion during his visit to IMECH, CAS. The computations were performed on resources provided by the National Supercomputing Center of Tianjin (NSCC-TJ).

Reference

1. Dublon IAN, Sumpter DJT. 2014 Flying insect swarms. *Curr. Biol.* **24**, R828–R830. (doi:10.1016/j.cub.2014.07.009)
2. Kelley DH, Ouellette NT. 2013 Emergent dynamics of laboratory insect swarms. *Sci. Rep.* **3**, 1073. (doi:10.1038/srep01073)
3. Breder CM Jr. 1951 Structure of a fish school. *B. Am. Mus. Nat. Hist.* **98**, 1–27.
4. Shaw E. 1970 *Development and evolution of behaviour*, pp. 452–480. San Francisco, CA: Freeman.
5. Lissaman PB, Shollenberger CA. 1970 Formation flight of birds. *Science* **168**, 1003–1005. (doi:10.1126/science.168.3934.1003)
6. Bajec IL, Heppner FH. 2009 Organized flight in birds. *Anim. Behav.* **78**, 777–789. (doi:10.1016/j.anbehav.2009.07.007)
7. Portugal SJ, Hubel TY, Fritz J, Heese S, Trobe D, Voelkl B, Hailes S, Wilson AM, Usherwood JR. 2014 Upwash exploitation and downwash avoidance by flap phasing in ibis formation flight. *Nature* **505**, 399–402. (doi:10.1038/nature12939)
8. Dombrowski C, Cisneros L, Chatkaew S, Goldstein RE, Kessler JO. 2004 Self-concentration and large-scale coherence in bacterial dynamics. *Phys. Rev. Lett.* **93**, 098103. (doi:10.1103/PhysRevLett.93.098103)
9. Zhang HP, Beer A, Florin EL, Swinney HL. 2010 Collective motion and density fluctuations in bacterial colonies. *Proc. Natl Acad. Sci. USA* **107**, 13 626–13 630. (doi:10.1073/pnas.1001651107)
10. Bricard A, Caussin JB, Desreumaux N, Dauchot O, Bartolo D. 2013 Emergence of macroscopic directed motion in populations of motile colloids. *Nature* **503**, 95–98. (doi:10.1038/nature12673)
11. Saintillan D, Shelley MJ. 2008 Instabilities and pattern formation in active particle suspensions: kinetic theory and continuum simulations. *Phys. Rev. Lett.* **100**, 178103. (doi:10.1103/PhysRevLett.100.178103)
12. Breder CM Jr. 1954 Equations descriptive of fish schools and other animal aggregations. *Ecology* **35**, 361–370. (doi:10.2307/1930099)
13. Weihs D. 1973 Hydrodynamics of fish schooling. *Nature* **241**, 290–291. (doi:10.1038/241290a0)
14. Weihs D 1975 Some hydrodynamical aspects of fish schooling in swimming and flying in nature. In *Swimming and flying in nature* (eds Theodore Y-T Wu, Charles J Brokaw, Christopher Brennen), vol. II, pp. 703–718. Springer.
15. Lopez U, Gautrais J, Couzin ID, Theraulaz G. 2012 From behavioural analyses to models of collective motion in fish schools. *Interface Focus* **2**, 693–707. (doi:10.1098/rsfs.2012.0033)
16. Breder CM Jr. 1967 On the survival value of fish schools. *Zoologica* **52**, 25–40.
17. Brock VE, Riffenburgh RH. 1960 Fish schooling: a possible factor in reducing predation. *ICES J. Mar. Sci.* **25**, 307–317. (doi:10.1093/icesjms/25.3.307)
18. Cushing DH, Jones FRH. 1968 Why do fish school? *Nature* **218**, 918–920. (doi:10.1038/218918b0)
19. Pitcher TJ, Magurran AE. 1982 Fish in larger shoals find food faster. *Behav. Ecol. Sociobiol.* **10**, 149–151. (doi:10.1007/BF00300175)
20. Breder CM Jr. 1965 Vortices and fish schools. *Zoologica* **50**, 97–114.
21. Belyayev VV, Zuyev GV. 1969 Hydrodynamic hypothesis of schooling in fishes. *J. Ichthyol.* **9**, 578–584.
22. Partridge BL, Pitcher TJ. 1979 Evidence against a hydrodynamic function for fish schools. *Nature* **279**, 418–419. (doi:10.1038/279418a0)
23. Partridge BL, Johansson J, Kalish J. 1983 The structure of schools of giant bluefin tuna in Cape Cod Bay. *Environ. Biol. Fish* **9**, 253–262. (doi:10.1007/BF00692374)
24. Hemelrijk CK, Reid D, Hildenbrandt H, Padding JT. 2015 The increased efficiency of fish swimming in a school. *Fish Fisheries* **16**, 511–521. (doi:10.1111/faf.12072)
25. Balchen JG. 1972 Feedback control of schooling fish. *IFAC Proc. Vol.* **5**, 511–518. (doi:10.1016/S1474-6670(17)68563-X)
26. Maertens AP, Gao A, Triantafyllou MS. 2017 Optimal undulatory swimming for a single fishlike body and for a pair of interacting swimmers. *J. Fluid Mech.* **813**, 301–345. (doi:10.1017/jfm.2016.845)
27. Novati G, Verma S, Alexeev D, Rossinelli D, van Rees WM, Koumoutsakos P. 2017 Synchronisation through learning for two self-propelled swimmers. *Bioinspir. Biomim.* **12**, 036001. (doi:10.1088/1748-3190/aa6311)
28. Verma S, Novati G, Koumoutsakos P. 2018 Efficient collective swimming by harnessing vortices through deep reinforcement learning. *Proc. Natl Acad. Sci. USA* **115**, 5849–5854. (doi:10.1073/pnas.1800923115)
29. Lighthill J. 1975 *Mathematical biofluid dynamics*. Philadelphia, PA: SIAM.
30. Zhu XJ, He GW, Zhang X. 2014 Flow-mediated interactions between two self-propelled flapping filaments in tandem configuration. *Phys. Rev. Lett.* **113**, 238105. (doi:10.1103/PhysRevLett.113.238105)
31. Becker AD, Masoud H, Newbolt JW, Shelley MJ, Ristroph L. 2015 Hydrodynamic schooling of flapping swimmers. *Nat. Commun.* **6**, 8514. (doi:10.1038/ncomms9514)
32. Ramananarivo S, Fang F, Oza A, Zhang J, Ristroph L. 2016 Flow interactions lead to orderly formations of flapping wings in forward flight. *Phys. Rev. Fluids* **1**, 071201(R). (doi:10.1103/PhysRevFluids.1.071201)
33. Zhu XJ, He GW, Zhang X. 2014 Numerical study on hydrodynamic effect of flexibility in a self-propelled plunging foil. *Comput. Fluids* **97**, 1–20. (doi:10.1016/j.compfluid.2014.03.031)
34. Shelton RM, Thornycroft PJ, Lauder GV. 2014 Undulatory locomotion of flexible foils as biomimetic models for understanding fish propulsion. *J. Exp. Biol.* **217**, 2110–2120. (doi:10.1242/jeb.098046)
35. Lucas KN, Thornycroft PJ, Gemmell BJ, Colin SP, Costello JH, Lauder GV. 2015 Effects of non-uniform stiffness on the swimming performance of a passively-flexing, fish-like foil model. *Bioinspir. Biomim.* **10**, 056019. (doi:10.1088/1748-3190/10/5/056019)
36. Ramananarivo S, Godoy-Diana R, Thiria B. 2013 Passive elastic mechanism to mimic fish-muscle action in anguilliform swimming. *J. R. Soc. Interface* **10**, 20130667. (doi:10.1098/rsif.2013.0667)
37. Liao JC, Beal BN, Lauder GV, Triantafyllou MS. 2003 Fish exploiting vortices decrease muscle activity. *Science* **302**, 1566–1569. (doi:10.1126/science.1088295)
38. Gray J. 1968 *Animal locomotion*. London, UK: Weidenfeld and Nicolson.
39. Ashraf I, Godoy-Diana R, Halloy J, Collignon B, Thiria B. 2016 Synchronization and collective swimming patterns in fish (*Hemigrammus bleheri*). *J. R. Soc. Interface* **13**, 20160734. (doi:10.1098/rsif.2016.0734)
40. Ashraf I, Bradshaw H, Ha TT, Halloy J, Godoy-Diana R, Thiria B. 2017 Simple phalanx pattern leads to energy saving in cohesive fish schooling. *Proc. Natl Acad. Sci. USA* **114**, 9599–9604. (doi:10.1073/pnas.1706503114)
41. Videler JJ. 1981 Swimming movements, body structure and propulsion in cod *Gadus morhua*. *Symp. Zool. Soc. London* **48**, 1–27.
42. McHenry MJ, Pell CA, Long JH. 1995 Mechanical control of swimming speed: stiffness and axial wave form in undulating fish models. *J. Exp. Biol.* **198**, 2293–2305.
43. Lauder GV, Lim J, Shelton R, Witt C, Anderson E, Tangorra JL. 2011 Robotic models for studying undulatory locomotion in fishes. *Mar. Technol. Soc. J.* **45**, 41–55. (doi:10.4031/MTSJ.45.4.8)
44. Wang SZ, Zhang X. 2011 An immersed boundary method based on discrete stream function formulation for two- and three-dimensional incompressible flows. *J. Comput. Phys.* **230**, 3479–3499. (doi:10.1016/j.jcp.2011.01.045)
45. Zhu XJ, He GW, Zhang X. 2014 An improved direct-forcing immersed boundary method for fluid–structure interaction simulations. *J. Fluid Eng.* **136**, 040903. (doi:10.1115/1.4026197)
46. Wang SZ, He GW, Zhang X. 2013 Parallel computing strategy for a flow solver based on immersed boundary method and discrete stream-function formulation. *Comput. Fluids* **88**, 210–224. (doi:10.1016/j.compfluid.2013.09.001)
47. Dai LZ, He GW, Zhang X. 2016 Self-propelled swimming of a flexible plunging foil near a solid wall. *Bioinspir. Biomim.* **11**, 046005. (doi:10.1088/1748-3190/11/4/046005)
48. Huang WX, Shin SJ, Sung HJ. 2007 Simulation of flexible filaments in a uniform flow by the immersed boundary method. *J. Comput. Phys.* **226**, 2206–2228. (doi:10.1016/j.jcp.2007.07.002)
49. Mckeown BA. 1984 *Fish migration*. London, UK: Croom Helm.